



Early chatter identification of robotic boring process using measured force of dynamometer

Guifeng Wang^{1,2} · Huiyue Dong¹ · Yingjie Guo¹ · Yinglin Ke¹

Received: 23 February 2017 / Accepted: 8 August 2017 / Published online: 25 August 2017
© Springer-Verlag London Ltd. 2017

Abstract The system of robotic boring, mainly involving an industrial robot and an end-effector, is prone to chatter during the boring process of intersection hole, which not only affects the machining surface quality, but also restricts the boring efficiency. To improve the quality and the efficiency of the intersection hole, a new approach to identify and forecast the chatter of a robotic boring system based on the measured force signal of the dynamometer is presented. The proposed approach consists of three steps. First, the measured force signal is decomposed a series of intrinsic mode functions (IMF) and a residue by empirical mode decomposition (EMD). Secondly, Hilbert transform is invoked for each IMF to obtain the instantaneous frequencies and the instantaneous magnitudes, which comprise the Hilbert-Huang spectrum of the original signal. Finally, the chatter feature is extracted by analyzing the Hilbert spectrum of each IMF and a statistical method is used to detect the chatter symptom. The experiment results show that the extracting chatter feature from the signal can gain the chatter symptom at most 0.6 s ahead of the chatter outbreak, which is beneficial to guarantee for follow-up chatter suppression and improve the surface quality of workpiece.

Keywords Robotic boring · Chatter · Empirical mode decomposition · Hilbert-Huang transform · Feature extraction

✉ Huiyue Dong
donghuiyue@zju.edu.cn

¹ The State Key Laboratory of Fluid Power and Mechatronic Systems, College of Mechanical Engineering, Zhejiang University, Hangzhou 310027, China

² School of mechanical and electrical engineering, Jinhua College of Profession and Technology, Jinhua 321007, China

1 Introduction

Robotic boring is an effective way to achieve the final machining of intersection holes [1]. However, compared with a standard machine tool, the chatter as a kind of self-excited instable vibration is more likely to happen than in the robotic boring system, which leads to a lower quality of final product surface, shorter tool life, and even tool or workpiece destruction [2]. Especially, the destruction brought by chatter will become more serious when the weak rigidity system is utilized to machine difficult-to-machine materials [3]. Thus, it is vital to identify and forecast the chatter of a robotic boring.

In chatter identification and forecast, the vibration signals that mostly reflect the state of machining are usually adopted to extract chatter feature. This way mainly includes two kinds of steps. One is to sample using sensors from these vibration signals such as acceleration signal [4–6], cutting force signal [7–9], sound signal [10, 11], motor current signal [12, 13], and torque signal [14], and the other is to extract chatter symptom from these signals using signal processing method. However, Fourier transform, as a common processing method, is not suitable for online detection of chatter onset, since chatter signal is a typical nonlinear and nonstationary signal. Thus, many new attempts have been made to adapt nonlinear and nonstationary signal processing, such as discrete wavelet transform and HHT [15, 16]. As a powerful time-frequency technique, the HHT has been widely used in the field of nonlinear and nonstationary signal processing. The original signals are first decomposed into a set of complete and almost orthogonal components based on a time nonstationary adaptive operation, and then a time-frequency distribution of the signals is obtained using Hilbert transform. Especially, the fault-tolerant ability and the discrimination speed of the forecasting system are significantly enhanced with the rapid development of artificial intelligence technology in recent years [17].

At present, only a few scholars focus on chatter identification and suppression of a robot machining system. Özer et al. [18] analyzed the delaying tool chatter in turning with a two-link robotic arm and found that the chatter can be greatly suppressed by varying the robot's joint stiffness. Mejri et al. [19] studied the dynamic behavior and machining stability of a robot system equipped with a high-speed machining spindle, and the result showed that the chatter can be significantly reduced by adjusting the robot's posture. However, there is almost no report about the chatter identification and forecast in the robotic boring. To improve the quality and the efficiency of the intersection hole in the robotic boring process, the chatter identification and forecast based on the measured force signal of a dynamometer is studied in this article. The vibration analysis and the measured force with pressure foot of the system are first presented. In Section 3, brief introductions of the EMD and the HHT are given. In Section 4, an experimental setup is introduced; next, the results and the analysis of the proposed identified method are given in Section 5. Finally, the conclusive remarks are laid out in Section 6.

2 Vibration analysis and measured force of the robotic boring

2.1 Vibration analysis

The robotic boring system is mainly comprised of an industrial robot, an end-effector, and a mobile platform. The robot is mounted on the mobile platform and the end-effector is attached to the end of the robot through the flange, which is

adopted to drive the feed and the rotational movements during the boring process. The coaxiality of the intersection hole and the boring bar is guaranteed by adjusting the robot pose. The schematic diagram of the pressure foot is shown in Fig. 1. The air cylinder is mounted on the either side of the end-effector and the pressure foot is driven by two air cylinders. When the pressure foot is drawn back, the boring process can be regarded as a periodic force applied on a cantilever beam. The vibration mechanism in this case has been studied in previous work [20]. The result shows that the forced vibration is dominant and the vibration frequency changes with the periodic frequency of the boring bar. Finally, it turns out that this type vibration can be largely suppressed by the pressure foot.

Once the pressure foot is pushed out, a pressure is applied on both the workpiece and the boring system under the action of the air cylinders, and the system transforms into a simply supported beam structure from a cantilever beam structure immediately, which leads to a remarkable growth of the stability and the stiffness of the system. In this case, chatter is often observed rather than the forced vibration. Furthermore, the frequency of the chatter is closed to the natural frequency of the boring bar, and whether it occurs largely depends on the robot posture [21]. The boring bar used is from the CK module of the KAISER tool, whose diameter and length are 31 and 135 mm, respectively. A modal test was performed to obtain the dynamic property of the boring bar. Three accelerometers evenly distributed on the boring bar were adopted to collect vibration signals. Based on the B&K PULSE testing analysis system, the frequency response of the boring bar was obtained as shown in Fig. 2. The result shows that its first order natural frequency is closed to 500 Hz.

Fig. 1 Schematic diagram of the pressure foot with (a) push out and (b) draw back

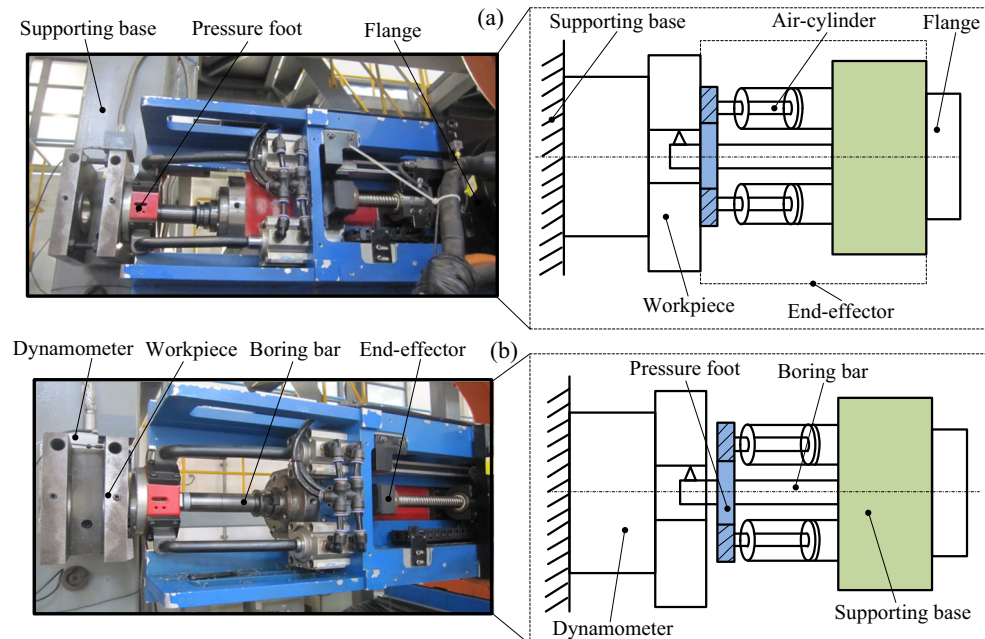
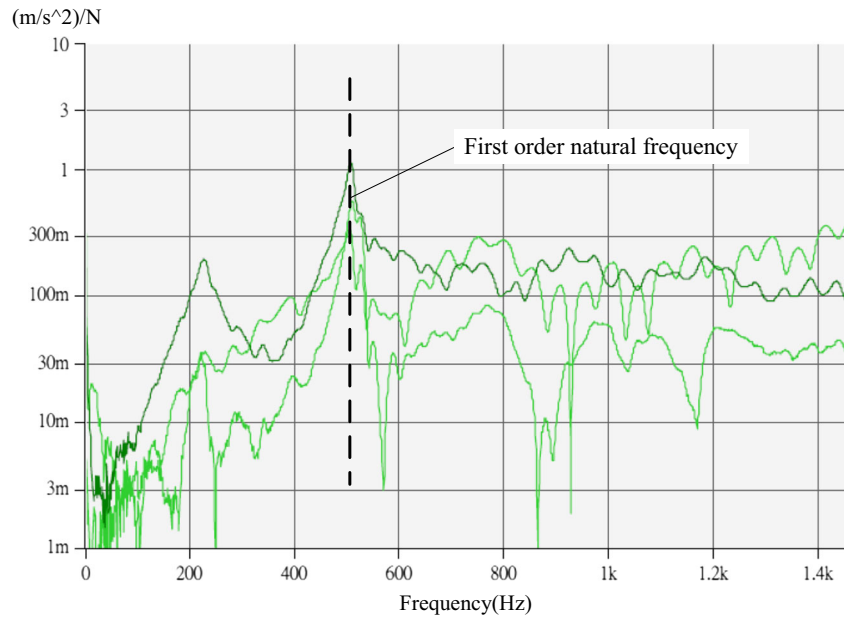


Fig. 2 Frequency response of the boring bar



2.2 Measured force of dynamometer

Also as shown in Fig. 1, the dynamometer is installed on the supporting base and the workpiece is mounted on the dynamometer. As mentioned above, the boring process can be regarded as a periodic force applied on a cantilever beam structure when the pressure foot is drawn back. Hence, in such a case, the measured force of the dynamometer equals the cutting force F . If the pressure foot is pushed out, due to the effect of friction force between the pressure foot and the workpiece, the measured force of dynamometer is equal to the resultant force of the cutting force F , the friction force caused by foot pressure F_{pf} , and the friction force caused by the barycenter movement of the motor F_{feed} , that is

$$F_{me} = F + F_{feed} + F_{pf} \quad (1)$$

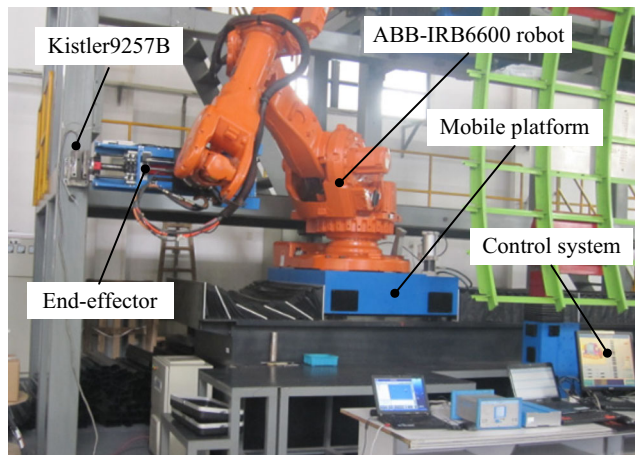


Fig. 3 Robotic boring experiment

The F_{pf} belongs to a static friction force whose direction depends on external force. The F_{feed} originates from the movement of the motor with direction parallel to the gravity, whose value can be obtained from the moment equilibrium principle. The analytic expression between the cutting force and the measured force of the dynamometer with foot pressure has been obtained in previous work [21].

3 Hilbert-Huang transformation

3.1 Empirical mode decomposition

Empirical mode decomposition (EMD) is a self-adaptive analysis method in which a complicated signal can be decomposed into a set of complete and almost orthogonal components designated as intrinsic mode function (IMF) [22]. Since the decomposition is based on the local characteristic time scale of the data, it is well suitable for nonlinear and nonstationary signals. Each IMF obtained from EMD can either be linear or nonlinear, and represents the intrinsic fluctuation of the signal with high frequency resolution. Besides, each IMF must satisfy two conditions: One is that, in the whole data set, the number of extrema and the number of zero crossings

Table 1 Geometrical parameters of the boring insert used in the boring experiment

| Nose radius | Inclination angle | End cutting edge angle | Side cutting edge angle | Rake angle |
|-------------|-------------------|------------------------|-------------------------|------------|
| 0.4 (mm) | − 7 (°) | 0 (°) | 30 (°) | 11 (°) |

Table 2 Boring variables and their setting levels in the robotic boring experiment

| Factors | Levels | | | | |
|--------------------------|--------|-------|-------|-------|-------|
| Rotational speed (r/min) | 200 | 300 | 400 | 600 | 800 |
| Feed rate (mm/r) | 0.05 | 0.075 | 0.1 | 0.15 | 0.2 |
| Depth of cut (mm) | 0.025 | 0.05 | 0.075 | 0.125 | 0.175 |
| Foot pressure (MPa) | 0 | 0.2 | 0.3 | 0.4 | 0.5 |

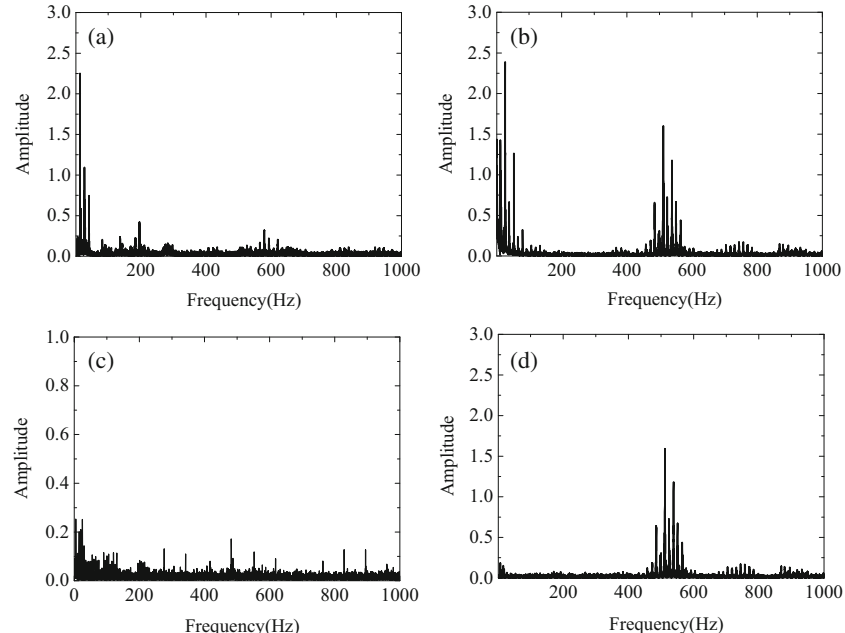
must either equal or differ at most by one. The other is that, at any point, the mean value of the envelope defined by the local maxima and the envelope defined by the local minima is zero [22]. Thus, for an arbitrary original signal $x(t)$, like the measured force signal of dynamometer, the obtained decomposition followed by the EMD method can be represented as

$$x(t) = \sum_{j=1}^n c_j(t) + r_n(t) \quad (2)$$

where n is the number of IMF, $c_i(t)$ is the i th IMF and $r_n(t)$ is the residue which indicates the central tendency of the original signal. The IMFs, $c_1(t), c_2(t), \dots, c_n(t)$, contain the characteristic scales of the original signal in different time scale and include different frequency bands ranging from high to low.

3.2 Hilbert-Huang transformation

HHT is a signal analysis method and was first proposed by Huang in 1998 [23]. It mainly consists of two steps: (1) by EMD, a complicated signal is first decomposed into a series of IMF, and (2) Hilbert transform is then invoked for each IMF to

Fig. 4 Four type amplitude-frequency curves from measured force of dynamometer**Table 3** The variables chosen from the orthogonal experiment

| Types | Depth of cut (mm) | Feed rate (mm/r) | Rotational speed (r/min) | Foot pressure (MPa) |
|---------|-------------------|------------------|--------------------------|---------------------|
| Stable | 0.05 | 0.05 | 300 | 0.3 |
| Chatter | 0.175 | 0.05 | 800 | 0.4 |

obtain the instantaneous frequencies and the instantaneous magnitudes, which comprise the Hilbert-Huang spectrum of the original signal [16]. Compared with the traditional signal processing methods, HHT has three advantages: (1) it gets rid of linearity limit and is suitable for the analysis of nonlinear and singular signals; (2) it has excellent adaptability; and (3) it is not subjected to the limit of Heisenberg uncertainty principle. Thus, this method is particularly fit for the measured force signal of the robotic boring.

The Hilbert Transform for IMF $c_i(t)$ can be written by

$$H[c_i(t)] = \frac{1}{\pi} P \int_{-\infty}^{+\infty} \frac{c_i(\tau)}{t-\tau} d\tau \quad (3)$$

where P is the Cauchy principal value and exists for all functions of class L^p . Supposing $c_i(t)$ and $H[c_i(t)]$ are complex conjugate pair, an analytic signal $a_i(t)$ can be given as

$$a_i(t) = c_i(t) + jH[c_i(t)] = A_i(t)e^{j\theta_i(t)} \quad (4)$$

in which

$$\begin{cases} A_i(t) = \sqrt{c_i^2(t) + H^2[c_i(t)]} \\ \theta_i(t) = \tan^{-1}\left(c_i(t)/H[c_i(t)]\right) \end{cases} \quad (5)$$

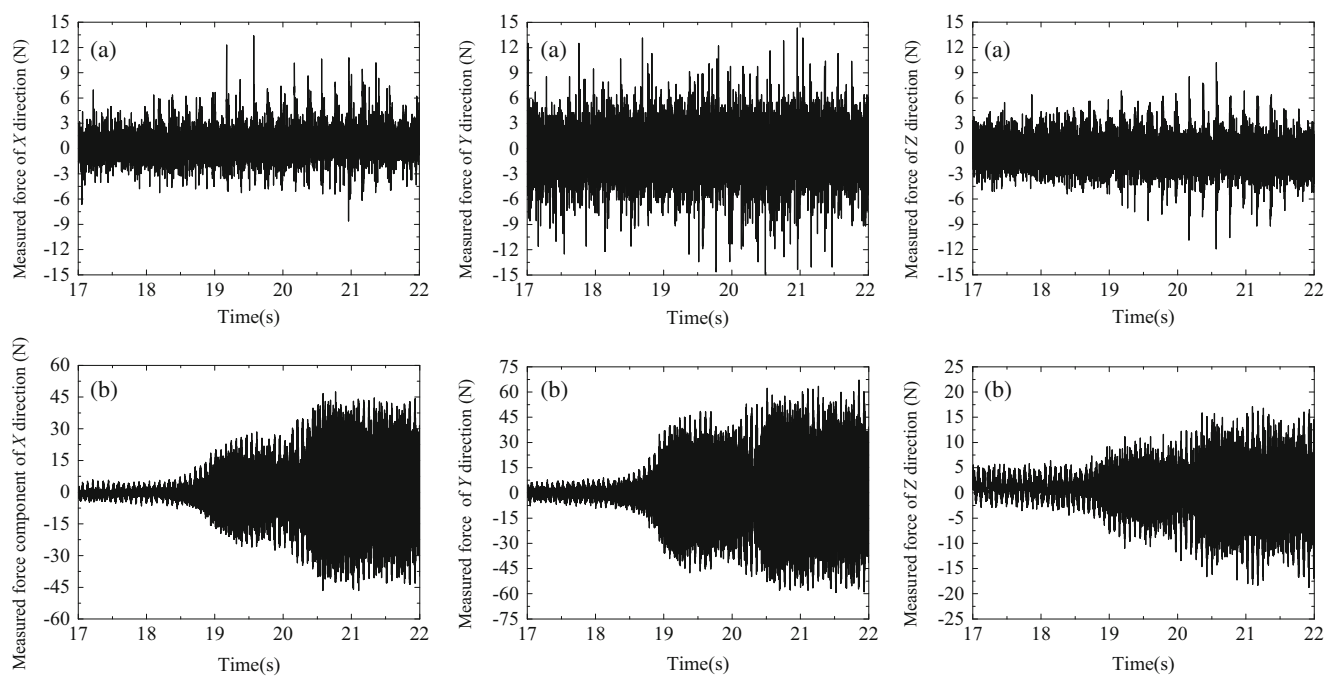


Fig. 5 Comparison of the measured force components for (a) stable boring and (b) chatter in 5 s

where $A_i(t)$ and $\theta_i(t)$ are the instantaneous amplitude and the instantaneous phase of $a_i(t)$, respectively. It is easy to know from Eq. 5 that the $A_i(t)$ and the $\theta_i(t)$ vary as a nonlinear function of the time. If the $\theta_i(t)$ is monocomponent, the instantaneous frequency $\omega_i(t)$ can be given as

$$\omega_i(t) = d\theta_i(t)/dt \quad (6)$$

Thus, the Hilbert-Huang spectrum of the original signal can be depicted as

$$H(\omega, t) = \text{Re} \sum_{i=1}^n A_i(t) e^{j\omega_i(t)dt} \quad (7)$$

where Re means the real component of complex number. It is clear from Eq. 7 that the time-frequency distribution of the

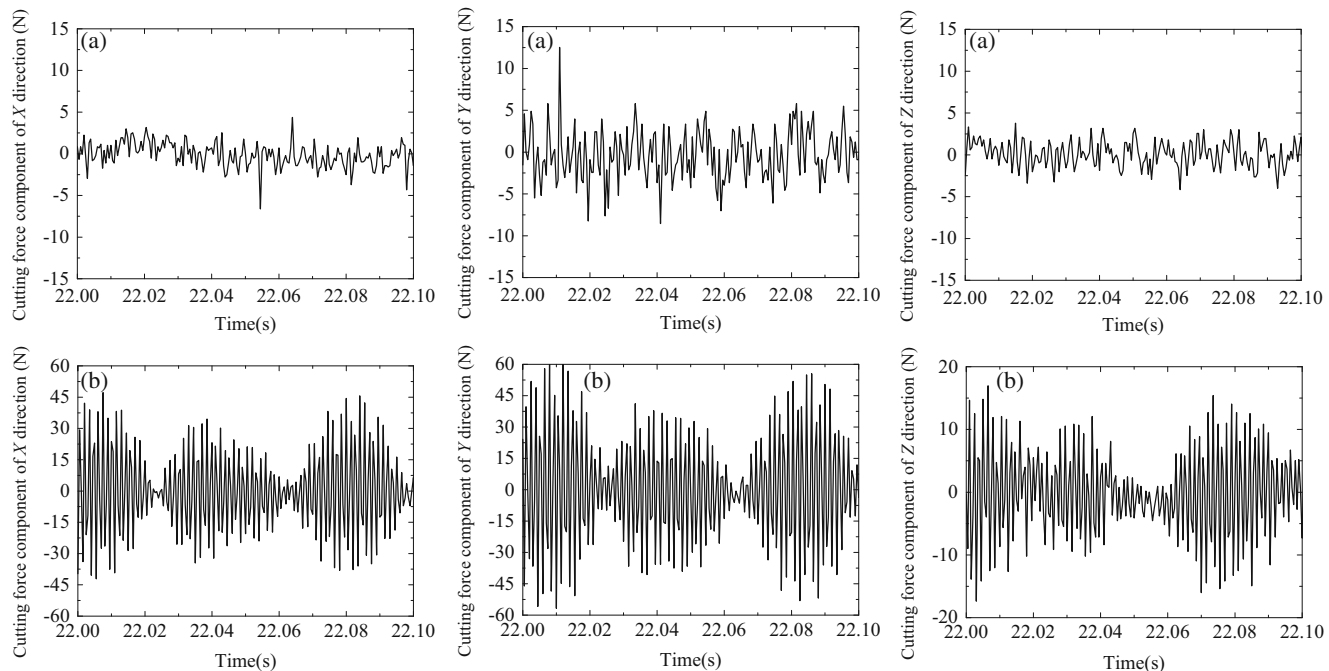


Fig. 6 Comparison of the measured force components for (a) stable boring and (b) chatter in 0.1 s

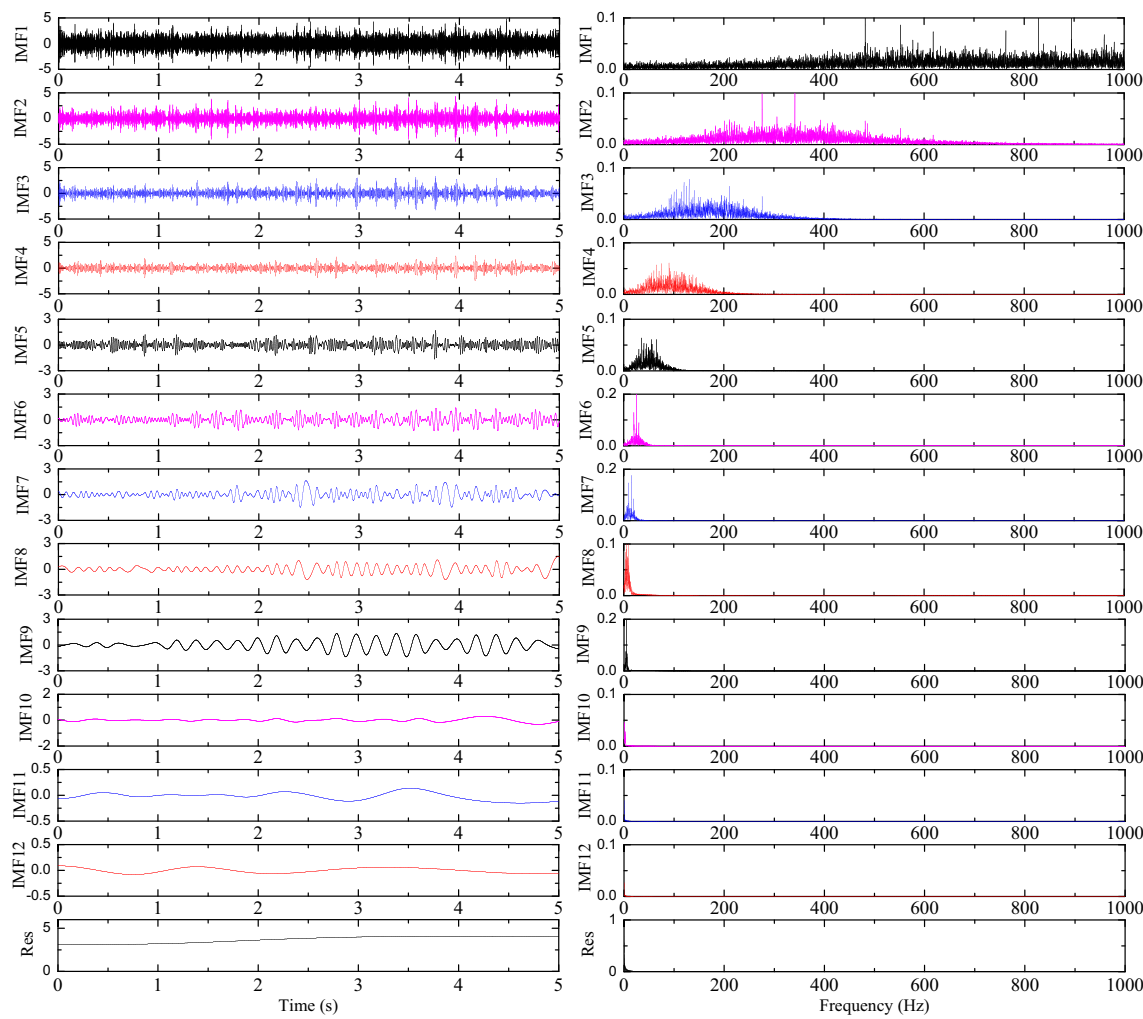


Fig. 7 IMFs and their corresponding amplitude-frequency curves of stable boring

amplitude can be easily acquired from the Hilbert-Huang spectrum. However, the amplitude and the frequency obtained by Fourier transform (FT) approach are blind to the variation of the time. Hence, the Hilbert transform can be regarded as a generalization of FT, while FT is a special case of the Hilbert transform.

4 Experiment setup

The experiments were conducted on an ABB IRB6600-175/2.55 with a self-designed end-effector, as shown in Fig. 3. The robot posture used in the experiment is $\theta_1 = -48.38$, $\theta_2 = 54.82$, $\theta_3 = 6.86$, $\theta_4 = -54.16$, $\theta_5 = 107.43$, and $\theta_6 = -21.95$. The material is high-strength steel. The geometrical parameters of the boring insert used in the experiment are listed in Table 1. A Kistler9257B dynamometer was used to measure the force generated during the boring with 2000 points per sampling frequency. To comprehensively analyze the variation of the measured force signal when chatter occurs, four factors

including the rotational speed (r/min), the feed rate (mm/r), the depth of cut (mm), and the foot pressure (MPa) are selected for the experiments. Five levels are chosen for each of them in the light of their actual range. Two orthogonal repeated experiments of $L_{25}(5^4)$ are performed, and the variables and their setting levels are as shown in Table 2. The surface of the work-piece was pre-processed before each test to eliminate the effect of the previous boring process and the foot pressure.

5 Result and analysis

All the measured force signals from the experiment were processed by fast Fourier transform, and a total of four type amplitude-frequency curves were found as shown in Fig. 4. The first type curve appeared when the pressure foot was drawn back as depicted in Fig. 4a. The frequency of the curve peak is not only closed to the periodic frequency of the boring bar, but also changes with it, so it is easy to see that the forced vibration in this case is dominant, such as when the machining

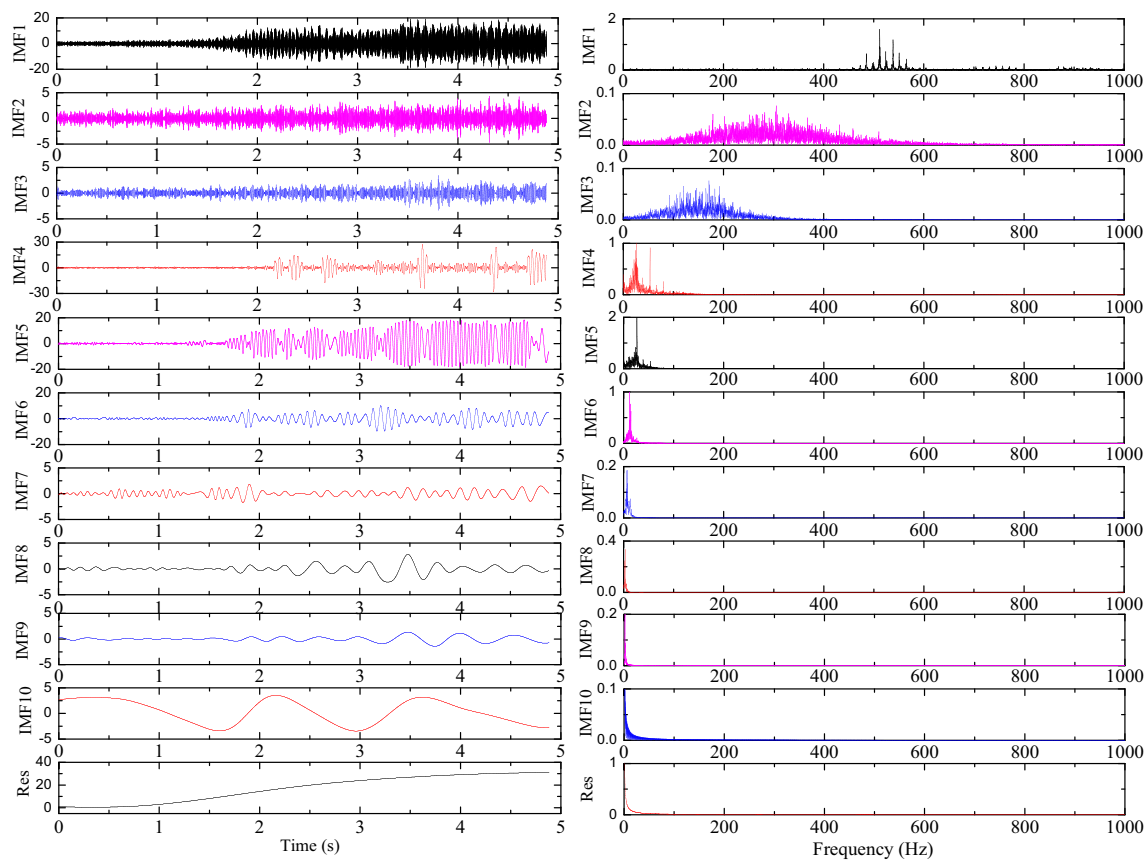


Fig. 8 IMFs and their corresponding amplitude-frequency curves when chatter occurs

parameters were $a_p = 0.025$ mm, $f = 0.05$ mm/r, $V_n = 200$ r/min, $P = 0$ MPa. As the foot pressure increased, the second type curve arose with two obvious curve peaks, as shown in Fig. 4b. The first curve peak is the same as the previous and is caused by the forced vibration. The frequency of the second curve peak is closed to the natural frequency of the boring bar. Since in the test it is only related to the dynamic performance of the boring system, this type of the vibration is identified as chatter, such as when the machining parameters were $a_p = 0.175$ mm, $f = 0.1$ mm/r, $V_n = 400$ r/min, $P = 0.2$ MPa.

Further, if the foot pressure is larger than 0.3 MPa, the third type curve appeared as shown in Fig. 4c. It is worth noting that the curve peak cannot be found in this figure, which means both the chatter and the forced vibration did not happen, such as when the machining parameters were $a_p = 0.05$ mm, $f = 0.05$ mm/r, $V_n = 300$ r/min, $P = 0.3$ MPa. This perfect boring state is just what we have been searching for. In order to achieve this state, both the sufficient foot pressure and the rational machining parameter must be guaranteed at the same time. The reason is that the forced vibration can be largely suppressed by the sufficient foot pressure and the rational

Fig. 9 Hilbert-Huang spectrum of the first IMF during (a) stable boring and (b) chatter

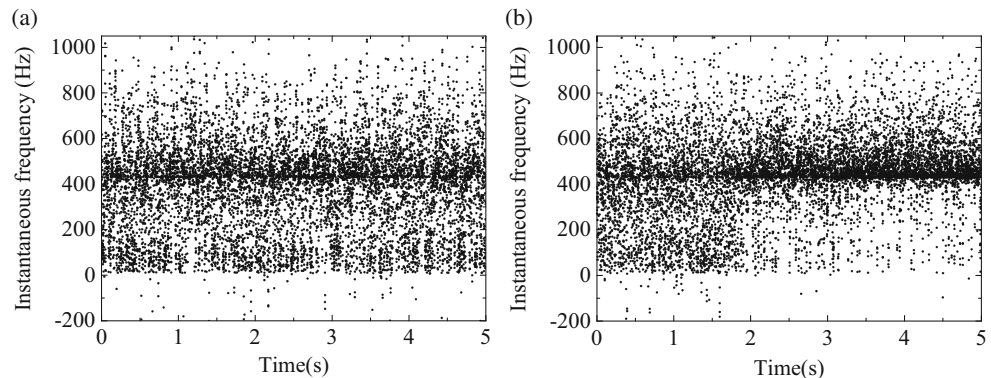
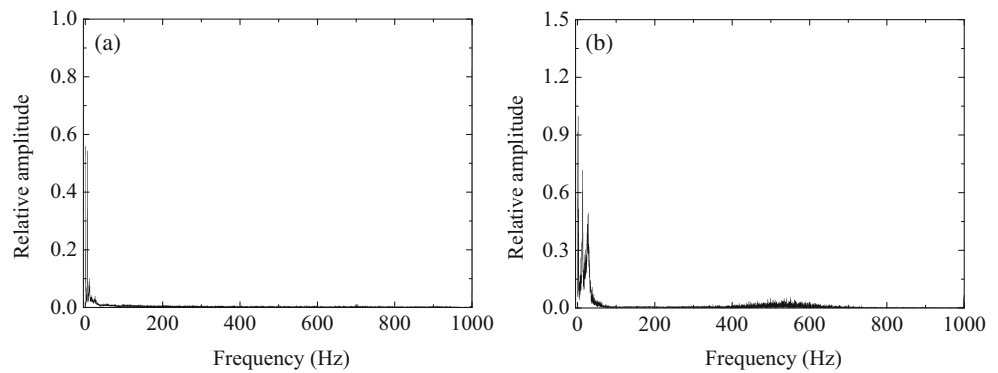


Fig. 10 Hilbert marginal spectrum of the first IMF during (a) stable boring and (b) chatter



cutting parameter is beneficial to maintain the stability of the system. With sufficient foot pressure, if the machining parameter continued to increase, the fourth type curve will occur as shown in Fig. 4d, such as when the machining parameters were $a_p = 0.175$ mm, $f = 0.05$ mm/r, $V_n = 800$ r/min, $P = 0.4$ MPa. The reason is that larger machining parameter reduces the stability of the system, and then makes the system give rise to chatter.

From the above analysis, an important conclusion can be drawn that a sufficient foot pressure and a rational machining parameter are essential for a stable boring. In order to suppress forced vibration to the maximum extent, sufficient foot pressure is usually the first thing to be guaranteed in the practice of the robotic boring. Thus, the third and fourth type curves are most likely to happen during the boring. For this reason, two of the measured forces, which are consistent with the third and the fourth type curves respectively, were chosen from the experiment to identify and forecast the chatter. Their variables are shown in Table 3.

Figure 5 shows a comparison of the measured force component from the two cases in 5 s. From the figure, it is easy to see that the measured force components almost remain the same when the boring is stable, but increase significantly until a dynamic equilibrium is reached when chatter occurs.

The curve of the measured force components is further presented in 0.1 s, as shown in Fig. 6. From the figure, it can be seen that the measured force components are almost unchanged with time when the boring is stable. The reason is

that the cutting force applied on the boring bar cannot be directly measured by the dynamometer due to the effect of the foot pressure. However, it varies dramatically with high frequency and sinusoidal period when chatter occurs. The high frequency originates from the chatter and the sinusoidal period is caused by fluctuant friction force between the work-piece and the pressure foot, which makes the effect of the cutting force on the dynamometer more obvious.

5.1 EMD of the measured force signal

Based on the principle of vector summation, the resultant force of the measured force components were first obtained, and then a series of IMFs was gained from the resultant force using EMD. Next, the amplitude-frequency curve of each IMF was obtained using fast Fourier transform. Figure 7 shows the IMFs of the resultant force and their amplitude-frequency curves when the boring is stable. It is clear from the figure that the resultant force signal is decomposed into 12 IMFs from high to low frequency. The frequency range of the first IMF is the highest with value more than 400 Hz; hence, its range is the most closest to the natural frequency of the boring bar. The frequency range from the fourth IMF to the seventh IMF is considered to have intimate relationship with the periodic frequency of the boring bar. By contrast each IMF, it is found that the amplitude of the first IMF is the largest, the second and the third IMFs followed by the others. Also, from the figure, it is easy to see that the relative peaks of

Fig. 11 The numbers of the instantaneous frequencies during (a) stable boring and (b) chatter

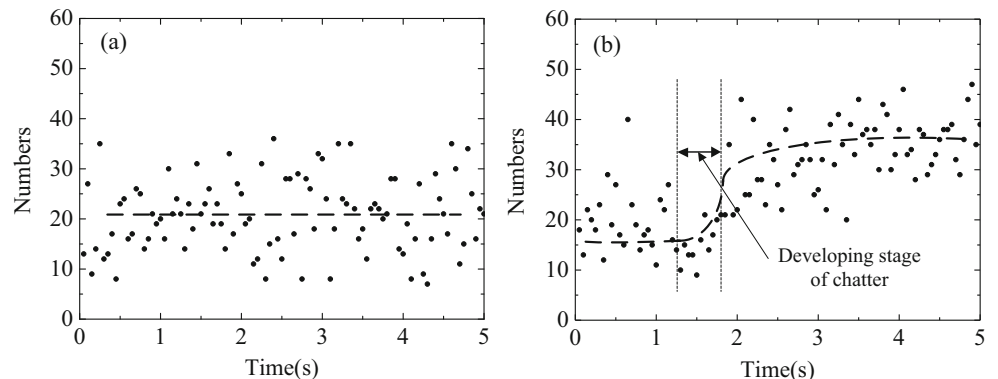
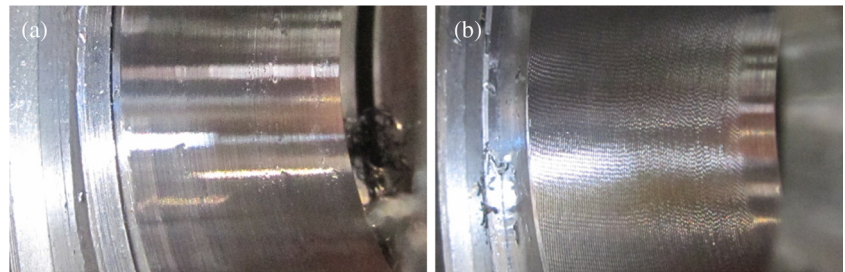


Fig. 12 Machined surface of the workpiece during (a) stable boring and (b) chatter



the amplitude-frequency curves are less than 0.2. In addition, the *Res* in the last row of the figure indicates the residue, whose amplitude-frequency curve is plotted on the right side.

Similarly, Fig. 8 shows the IMFs of the resultant force and their amplitude-frequency curves when the chatter occurs. From the figure, it is clear that the resultant force signal is decomposed into 10 IMFs and the amplitude of the IMFs is entirely increased in contrast with previous stable boring. Especially, the amplitude of the first IMF grows rapidly until a new equilibrium is reached, which means the first IMF has the greatest amount of energy. Their amplitude-frequency curves are also increased by comparing the stable boring. It is obvious that the first IMF's amplitude-frequency curve appeared with maximum amplitude, which means that chatter occurs since its frequency range is closed to the natural frequency of the boring bar. Similarly, the peaks of the fifth IMF, the sixth IMF, and the seventh IMF also become larger with a smaller increment. Because their frequency ranges are closed to the periodic frequency of the boring bar, it can be drawn that this is caused by the forced vibration with a less effect under the action of the pressure foot. Other peaks of the curves that are almost unchanged when chatter occurs are related to the dynamic performance of the system.

5.2 HHT of the measured force signal

HHT was further performed on each IMF to obtain the Hilbert-Huang spectrum. By comparing the Hilbert-Huang spectrum of each IMF, it was found that the variation of the first IMF is most obvious when chatter occurs. From the viewpoint of energy, this variation was generated by the self-excited vibration between the tool and the workpiece. Therefore, the first IMF can be regarded as the subject to identify the chatter of robotic boring with the greatest amount of energy. Figure 9 shows a comparison of the first IMF's Hilbert-Huang spectrum between the stable boring and the chatter. It can be seen from the figure that the instantaneous frequency basically remains unchanged over time during the stable boring, but varies from low to high at the time of the chatter outbreak. After that, the chatter frequency is mainly focused on 500 Hz, which means the system gradually reaches a dynamic equilibrium. It is worth noting that this is adverse to the situation when chatter occurs in a standard machine tool

system, whose vibration frequency varies from high to low during the chatter outbreak [8]. The reason is that vibration frequency when chatter occurs is usually closed to the natural frequency of the machining system, thus for a standard machine tool system with low natural frequency, its vibration frequency varies from high to low during chatter outbreak. However, this may not be suitable for the robotic boring system due to its special structure, because its vibration frequency when chatter occurs nears to the natural frequency of the boring bar, which leads to vibration frequency varied from low to high.

Figure 10 shows the Hilbert marginal spectrum of the first IMF of the two cases. From the figure, two curve peaks can be easily found near the range of the periodic frequency and the natural frequency of the boring bar, which further verify that the forced vibration frequency equals the periodic frequency of the boring bar and the chatter frequency is closed to the natural frequency of the boring bar.

5.3 Chatter identification

To further study the variation of the frequency before and after the chatter, the first IMF's Hilbert-Huang spectrum was analyzed using statistical method. The numbers of the frequencies in the range of 450–600 Hz for every 100 samples was calculated along with the time, as shown in Fig. 11. From the figure, it can be seen that the numbers of the frequencies start to increase during the early stage of the chatter, while almost remains unchanged over time when the boring is stable. Also, it is obvious from the figure that the developing stage is about 0.5~0.6 s and the numbers of frequencies increase from about 20 to more than 30. Using this difference, a chatter symptom can be gained at most 0.6 s ahead of the chatter outbreak, which is beneficial to guarantee for follow-up chatter suppression and improve the surface quality of workpiece.

Figure 12 shows the machined surface of the workpiece between the stable boring and the chatter. From the figure, it is clear for the stable boring that the machined surface is smooth with high quality, but shows apparent vibration marks with high frequency when chatter occurs, which is closely related to the chatter frequency of the system.

6 Conclusions

Using EMD and HHT, this paper presents a new approach to identify and forecast the chatter of a robotic boring system based on the measured force signal of the dynamometer. The proposed approach was verified through twice orthogonal experiments and the results have shown that (1) by FFT on the measured force signal, it is further verified that the frequency of the forced vibration equals the periodic frequency of the boring bar and the chatter frequency is closed to the natural frequency of the boring bar; (2) both the sufficient foot pressure and the rational machining parameter are essential for a stable boring; (3) the first IMF's Hilbert-Huang spectrum is most obvious at the time of the chatter outbreak; (4) different from a standard machine tool system whose vibration frequency varies from high to low, the vibration frequency of a robotic boring system varies from low to high when chatter occurs; and (5) by extracting the chatter feature from the first IMF's Hilbert-Huang spectrum, a chatter symptom can be gained at most 0.6 s ahead of the chatter outbreak, which is beneficial to guarantee for follow-up chatter suppression.

Acknowledgements This research was supported by the National Natural Science Foundation of China (No.: 51575479) and the Science Fund for Creative Research Groups of National Natural Science of Foundation of China (No.: 51521064).

References

- Wang G, Dong H, Guo Y, Ke Y (2016) Dynamic cutting force modeling and experimental study of industrial robotic boring. *Int J Adv Manuf Technol* 86:179–190
- Rusinek R, Lajnert P, Kecik K, Kruszynski B, Warminski J (2015) Chatter identification methods on the basis of time series measured during titanium super alloy milling. *Int J Mach Tools Manuf* 99: 196–207
- Pan Z, Zhang H, Zhu Z, Wang J (2006) Chatter analysis of robotic machining process. *J Mater Process Technol* 173:301–309
- Lamraoui M, Thomas M, ElBadaoui M (2014) Cyclostationarity approach for monitoring chatter and tool wear in high speed milling. *Mech Syst Signal Process* 44(1–2):177–198
- Shao Y, Deng X, Yuan Y, Mechefske CK, Chen Z (2014) Characteristic recognition of chatter mark vibration in a rolling mill based on the non-dimensional parameters of the vibration signal. *J Mech Sci Technol* 28(6):2075–2080
- Hynynen KM, Ratava J, Lindh T, Rikkonen M, Rynnänen V, Lohtander M, Varis J (2014) Chatter detection in turning processes using coherence of acceleration and audio signals. *J Manuf Sci Eng* 136(4):044503
- Lamraoui M, Thomas M, ElBadaoui M, Girardin F (2014) Indicators for monitoring chatter in milling based on instantaneous angular speeds. *Mech Syst Signal Process* 44(1–2):72–85
- Tangjitsitcharoen S, Saksri T, Ratanakuakangwan S (2013) Advance in chatter detection in ball end milling process by utilizing wavelet transform. *J Intell Manuf* 26(3):1–15
- Huang P, Li J, Sun J, Zhou J (2012) Vibration analysis in milling titanium alloy based on signal processing of cutting force. *Int J Adv Manuf Technol* 64(5–8):613–621
- Nair U, Krishna BM, Namboothiri VNN, Nampoori VPN (2010) Permutation entropy based real-time chatter detection using audio signal in turning process. *Int J Adv Manuf Technol* 46(1):61–68
- Thaler T, Potočnik P, Bric I, Govekar E (2014) Chatter detection in band sawing based on discriminant analysis of sound features. *Appl Acoust* 77:114–121
- Liu H, Chen Q, Li B, Mao X, Mao K, Peng F (2011) On-line chatter detection using servo motor current signal in turning. *Sci China Technol Sci* 54(12):3119–3129
- Liu Y, Wang X, Lin J, Zhao W (2016) Early chatter detection in gear grinding process using servo feed motor current. *Int J Adv Manuf Technol* 83:1801–1810
- Tansel IN, Li M, Demetgul M, Bickraj K, Kaya B, Ozcelik B (2010) Detecting chatter and estimating wear from the torque of end milling signals by using Index Based Reasoner (IBR). *Int J Adv Manuf Technol* 58(1–4):109–118
- Yao Z, Mei D, Chen Z (2010) On-line chatter detection and identification based on wavelet and support vector machine. *J Mater Process Tech* 210:713–719
- Senroy N, Suryanarayanan S, Ribeiro PF (2007) An improved Hilbert-Huang method for analysis of time-varying waveforms in power quality. *IEEE Trans Power Syst* 22(4):1843–1850
- Lamraoui M, Barakat M, Thomas M, Badaoui ME (2015) Chatter detection in milling machines by neural network classification and feature selection. *J Vib Control* 2(7):1251–1266
- Özer A, Semercigil SE, Kumar RP, Yowat P (2013) Delaying tool chatter in turning with a two-link robotic arm. *J Sound Vib* 332: 1405–1417
- Mejri S, Gagnol V, Le TP, Sabourin L, Ray P, Paultre P (2016) Dynamic characterization of machining robot and stability analysis. *Int J Adv Manuf Technol* 82:351–359
- Guo Y, Dong H, Wang G, Ke Y (2016) Vibration analysis and suppression in robotic boring process. *Int J Mach Tools Manuf* 101:102–110
- Wang G, Dong H, Guo Y, Ke Y (2017) Chatter mechanism and stability analysis of robotic boring. *Int J Adv Manuf Technol* 91: 411–421
- Cao H, Lei Y, He Z (2013) Chatter identification in end milling process using wavelet packets and Hilbert–Huang transform. *Int J Adv Manuf Technol* 69:11–19
- Huang N E, Shen Z, Long S R, Wu M C, Shih H H, Zheng Q, Yen N C, Tung C C, Liu H H (1998) The empirical mode decomposition and the Hilbert spectrum for nonlinear and non-stationary time series analysis. *Proc R Soc Lond A Math Phys Eng Sci* 454:903–995